the problems of aircraft motion will likely be less important than in the present study. This SAR device, if rigged on an orbiting platform, might be subject to fewer problems than experienced on the aircraft. If this were done, the interferometer technique might make feasible the remote sensing of the surface current field for the world oceans.

REFERENCES AND NOTES

1. R. M. Goldstein and H. A. Zebker, *Nature* **328**, 707 (1987).
2. F. I. Gonzales, C. L. Rufenbach, R. A. Shuchman, in *Oceanography from Space*, J. F. R. Gower, Ed. (Plenum, New York, 1981), pp. 511–523.
3. R. K. Raney, *IEEE Trans. Aerosp. Electron. Syst.* **AES-7**, 499 (1971).
4. SAR theory is described in R. Stewart, *Methods of Satellite Oceanography* (Univ. of California Press, Berkeley, 1985), p. 352.
5. Bragg waves observed by the SAR most effectively feel currents at a depth of approximately 2 cm below the mean surface [R. Stewart and J. Joy, *Deep Sea Res.* **21**, 1039 (1974)]. We measured these (very) near-surface currents with drifting pieces of plywood (1.2 m long by 0.6 m wide by 2 cm thick) with an identification number on the top. Their overall horizontal dimensions made them rather insensitive to vertical motions of the short waves, whereas their thickness ensured response to the very near-surface currents felt by the Bragg waves. The windage of these simple floats was virtually nil, a fact we checked by droguing several buoys with large, 20-liter, water-filled plastic bags.
6. The research described in this paper was carried out, in part, by the Jet Propulsion Laboratory (JPL) of the California Institute of Technology and was sponsored by JPL and the Defense Advanced Research Projects Agency through an agreement with the National Aeronautics and Space Administration. The University of California Space Institute and the Scripps Institution of Oceanography also sponsored this work. We thank B. and W. Barnett, D. Fuhrman, and A. Saraspe for assisting with the ocean portion of the field program.

17 July 1989; accepted 28 September 1989

Magnitude of Late Quaternary Left-Lateral Displacements Along the North Edge of Tibet

GILLES PELTZER,* PAUL TAPPONNIER, ROLANDO ARMIJO

Images taken by the earth observation satellite SPOT of the Quaternary morphology at 18 sites on the 2000-kilometer-long Altyn Tagh fault at the north edge of Tibet demonstrate that it is outstandingly active. Long-term, left-lateral strike-slip offsets of stream channels, alluvial terrace edges, and glacial moraines along the fault cluster between 100 and 400 meters. The high elevation of the sites, mostly above 4000 meters in the periglacial zone, suggests that most offsets resulted from slip on the fault since the beginning of the Holocene. These data imply that slip rates are 2 to 3 centimeters per year along much of the fault length and support the hypothesis that the continuing penetration of India into Asia forces Tibet rapidly toward the east.

FOR NEARLY 2000 KM, THE ALTYN Tagh fault follows the northwestern edge of the Tibet-Qinghai highlands (Fig. 1). From studies of Landsat images, the fault has been inferred to be active, left-lateral (*1, 2*), and to absorb an important fraction of the present-day convergence between India and Asia by allowing the Tibet-Qinghai plateau to move northeastward relative to the Tarim basin (*1*). Little else is known of this fault, however. The historical seismic record in its vicinity is scanty (*3*). Strike-slip surface breaks have been found in the field only at two localities, near 90° and 96°E (*4*). Estimates of the rate of horizontal slip on the fault vary widely (*5*). Thus, although the length and morphology of the Altyn Tagh fault (*6*) imply that it may be the largest Quaternary strike-slip fault of Asia, further constraints on the amount and history of recent movement are required for a quantitative understanding of recent tectonics north of the Himalayas.

Laboratoire de Tectonique, Mécanique de la Lithosphère, Institut de Physique du Globe de Paris, 4, place Jussieu, 75252 Paris, Cedex 05, France.

*Now at Jet Propulsion Laboratory, California Institute of Technology, Pasadena, CA 91109.

With a pixel size of 10 m in the panchromatic mode, images taken by the satellite SPOT (*7*) allow identification of cumulative Holocene offsets (that is, of features ~10,000 years old) on all faults moving at rates faster than 1 mm per year. In order to measure long-term offsets of late Quaternary morphological features and deposits along the Altyn Tagh fault, we studied seven scenes selected on the basis of earlier work with Landsat (*1*). In these scenes, late Quaternary deformation is spectacular at 18 sites (Fig. 1), 11 of which allow unambiguous estimates of recent left-lateral offsets (Table 1). We describe some of these sites below.

At site 1, the fault trace is marked in abundant, hummocky glacial till. It cuts the valley of a glacier and offsets its lateral moraines (Fig. 2, A and B). The left-lateral offset of the eastern, well-preserved, moraine ridge is 100 ± 20 m. The tip of the present glacier tongue in the valley lies only 1750 m upstream from the fault trace, thus only a few hundred meters above it if the valley slope is 10 to 20% (Fig. 2, A and B).

Between 78° and 79°E, the fault trace lies in the Karakax He valley, for the most part above 4000 m (Fig. 1). Here this valley is a gently west-sloping trough, several kilometers wide, flanked on either side by high mountains, which have been dissected by numerous, mostly extinct valley glaciers (*8*). Streams now flowing down such valleys north of the Karakax have built large alluvial fans. On the SPOT images, the fan deposits appear to form three major terraces, which are cut by the fault trace (Fig. 2, C to F). At site 3 (Fig. 2, C and D), for instance, the edges of the upper and middle terraces on the east bank of the stream are offset left-laterally by 185 ± 20 m. At sites 5 and 6 (Fig. 1 and 2, E and F), two ancient fans are offset 210 ± 20 m and 240 ± 20 m, respectively, in a left-lateral sense. The upper surfaces of these fans are incised by small channels and are no longer depositional surfaces (Fig. 2, E and F). The height of the fan surfaces above the Karakax flood plain and their degree of erosion suggest that they correspond to the middle terrace level at site 3 (Fig. 2, B and D). Close examination of the SPOT image reveals that the fault scarp in the fan surface at site 5 (Fig. 2E) faces toward the north across the eastern half of the fan and toward the south across the western half of this fan (*9*). This geometry, which is also clear across the fan at site 6 and across the terraces at site 3, attests to

Table 1. Values of 15 late Quaternary offsets measured along the Altyn Tagh fault. Errors are taken to be ±2 pixels [pixel sizes are 10 m and 20 m for panchromatic and multispectral (XS) images, respectively] for offsets of sharp, fossil morphological features (for example terrace or moraine edges), and standard deviations for average offsets of stream channels. Approximate elevations of sites, from (*6*), and inferred ages of offsets are also indicated.

Site	Offset (m)	Elevation (m)	Age (10^3 years)
1	100 ± 20	5000	<8
2	175 ± 20	4000	10 ± 2
3	185 ± 20	4000	10 ± 2
	185 ± 20		
5	210 ± 20	4000	10 ± 2
6	240 ± 20	4000	10 ± 2
7	~120	4000	<12
	~250		
	~120		
10	250 ± 80	4600	?
11	195 ± 95	3600	10 ± 2 ?
13	~400	4400	10 ± 2 ?
15	125 ± 40	3500	<8 ?
	125 ± 40		
18	60 ± 40	3300	10 ± 2 ?

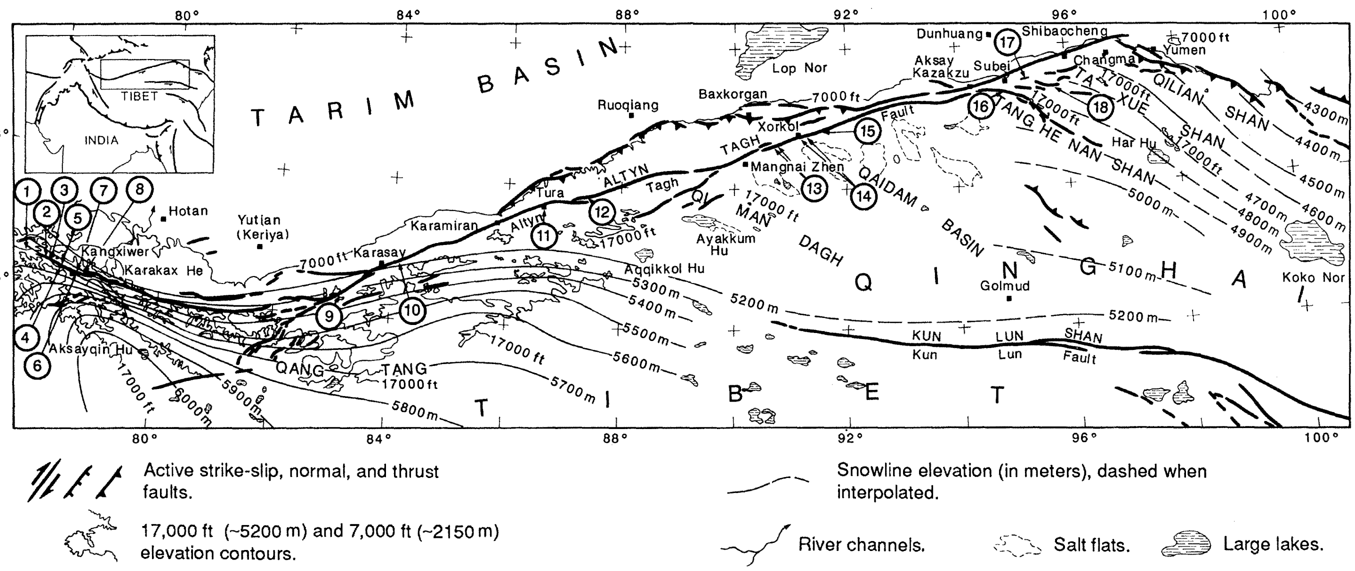

Fig. 1. Map of northern boundary of Tibet-Qinghai highlands along Tarim basin. Altyn Tagh fault roughly follows this boundary. Numbers refer to sites discussed in text.

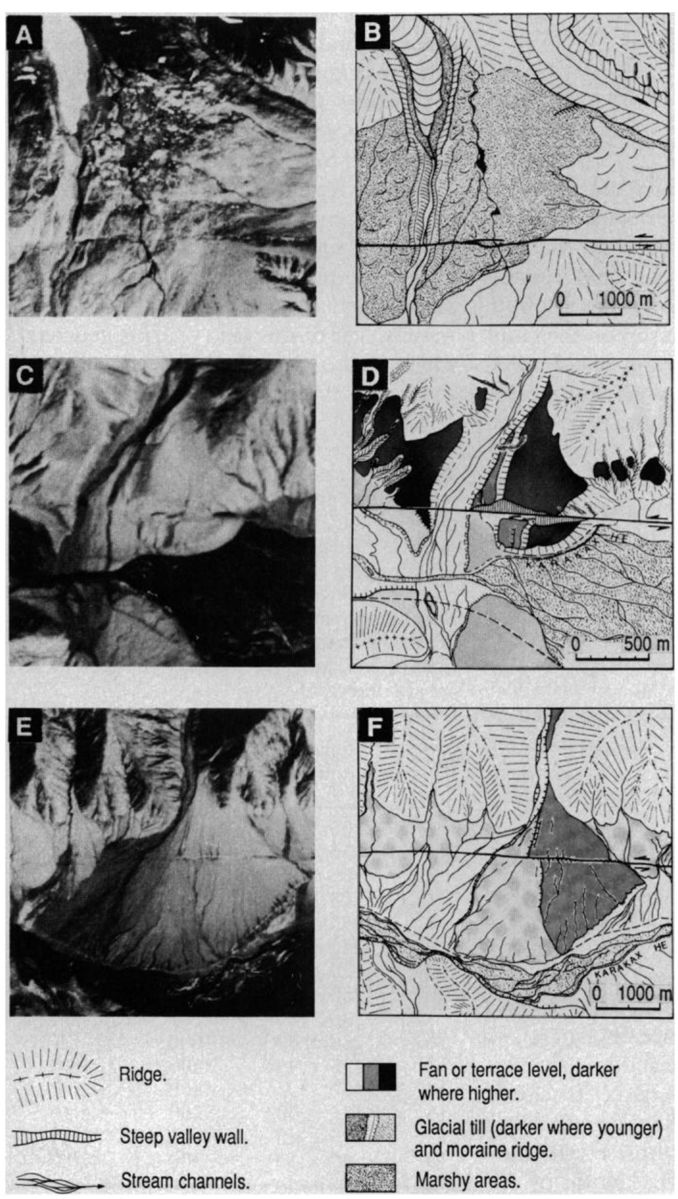

Fig. 2. Images (**A, C, E**) and corresponding sketch maps (**B, D, F**) of offset Quaternary fans in Karakax river valley, and of offset moraine in high area west of it (A, C, and E correspond to sites 1, 3, and 5, respectively on figure 1). Panchromatic SPOT scenes KJ 204–277 and 205–277. North is up.

nearly pure strike-slip on the fault and results from the conical shape of the alluvial fan surfaces.

Comparable left-lateral offsets occur at other sites along the Karakax valley: at site 2, a small valley floored by a terrace corresponding to the middle terrace at site 3 is offset by 175 ± 20 m, and at site 7, the fault offsets three transverse ridges by 120, 255, and 120 m (Fig. 1 and Table 1) (*10*).

The Karakax valley segment also offers outstanding examples of surface deformation compatible with late Quaternary left-lateral movement. Both a ~1100 by 100-m push-up anticline in a compressional jog at site 4 and a ~700 by 100-m pull-apart basin in a dilational jog at site 8 (Fig. 1) (*10*) have extremely youthful morphology and deform alluvial deposits apparently coeval with the fans at sites 5 and 6, and with the middle terrace at site 3 (Fig. 2, C to F). We infer that these structures are still growing. Their dimensions suggest that they result from displacements on the order of those measured at sites 2, 3, 5, and 6 (175 to 240 m, Table 1).

At sites 10 and 11 the courses of tributaries of major rivers such as the Qargan He (Figs. 1 and 3) are all disrupted along the fault trace. The geometry of most trailing streams attests to left-lateral movement. At site 11 (Fig. 3), a prominent shutter ridge deviates all stream channels: 21 measurements of left-lateral offsets made along the 20-km-long fault segment shown average 195 ± 95 m (Table 1). Similarly at site 10, 13 measurements of left-lateral stream offsets along a 20-km-long segment average 250 ± 80 m (Table 1) (*10*). In contrast with the fossil moraines or fans offset along the Karakax segment of the fault, the deviated channels at these sites still evolve under the action of seasonal drainage. We infer that this evolution is one cause of the greater dispersion of the offset values measured here (Table 1, Fig. 3).

At site 13 the fault has truncated the head of a large fan and isolated it from its source; the southwest edge of this now fossil fan has been offset by about 400 m (*10*). At site 15 (Figs. 1 and 4A), SPOT images reveal the remarkable linearity and continuity of the fault trace in a narrow, flat-floored trough, previously inferred with Landsat to represent evidence of active faulting (*1*). Here, as along the Karakax valley, the fault trace traverses Quaternary sediments; it is marked by long narrow ridges, or small push-up anticlines, and pull-apart basins (1 and 2, respectively, on Fig. 4A) that indicate left-lateral strike-slip movement. Adjacent to a pull-apart basin, the distal, lobate edge of a small fan, which is outlined by white silt, is offset 125 ± 40 m by the fault (arrows 3 on Fig. 4A). About 8 km east of this pull-apart basin, the eastern, lateral edge of a large fan, also outlined by silt, is offset left-laterally by the same amount (*10*).

East of Aksay Kazaksu, several faults splay from the main branch of the Altyn Tagh fault, which continues toward the northeast with a constant strike. SPOT images reveal that all these faults, which follow the more easterly or southeasterly trending ranges of the Tang He Nan and Ta Xue Shan, are active, strike-slip faults, and their traces cut across all Quaternary deposits and surfaces (sites 16 and 17, Fig. 1). One such fault is the Shibaocheng-Changma fault, north of the Ta Xue Shan (*11*). South of this fault, at an elevation of about 3300 m between the two ranges (site 18, Fig. 1), another splay-fault offsets a dense network of small, north-south erosion channels that incise loess-covered fossil fan surfaces (Fig. 4B). Here, measurement of individual channel offsets is difficult, partly because their spacing is on the order of a few tens of meters, almost the resolution of the image. The left-lateral offset of the right bank of one of the wider, flat-floored stream valleys that drain north into the Tang He is clear, however (1 on Fig. 4B), and amounts to 60 ± 40 m.

Because the Altyn Tagh fault runs across remote areas, the surface deformations described above have not been targets of detailed fieldwork. Hence, we cannot determine the ages of the various offsets on the basis of direct evidence concerning the stratigraphy and chronology, even relative, of Quaternary deposits near the fault. That much of the fault trace lies above 3000 m and that most of the sites are located less than 1500 m below the present snowline, however (Fig. 5), allows inferences to be drawn, by comparison, from studies of the Quaternary geology and climates in the region (*11–13*). In this region, major changes in erosion or sedimentation rates and surface morphology seem to have been intimately tied to major glacial pulses (*13*). Of particular importance are the onsets of warm interglacials, which are now known from ^{18}O isotope studies in the world oceans (*14*) to have been rapid, global instabilities. In Tibet, the frontal moraines of extinct glaciers and the highest levels of shorelines ringing large lakes appear to be of early Holocene age (*13*). At an elevation of about 4000 m, the Karakax segment of the Altyn Tagh fault must have been in the periglacial zone during much of the Würm glacial period, when the snowline was more than 500 m below its present position (about 5300 m, Figs. 1 and 5) (*11–13*). Furthermore, the area covered by hummocky, fresh till around site 1, at 5000 m, must have been under ice. Hence, the lateral moraine of the active glacier at site 1 is most likely only a few thousand years old and in any case distinctly younger than 8000 years old (*15*). Therefore, we infer that the 100-m offset of this moraine occurred during the last 8000 years (Table 1). The formation of the large fans in the Karakax valley most likely postdates the onset of the Holocene, because important deposition by rivers is unlikely to have occurred during the Würm glacial period at such elevations. Moreover, the small number and reduced size of present glaciers, together with the traces of widespread recent glacial imprint in the mountains above the valley, suggest that the fans formed from increased runoff at the beginning of the Holocene. If this hypothesis is correct, then the offsets of the fans and terrace edges at sites 3, 5, and 6 must postdate

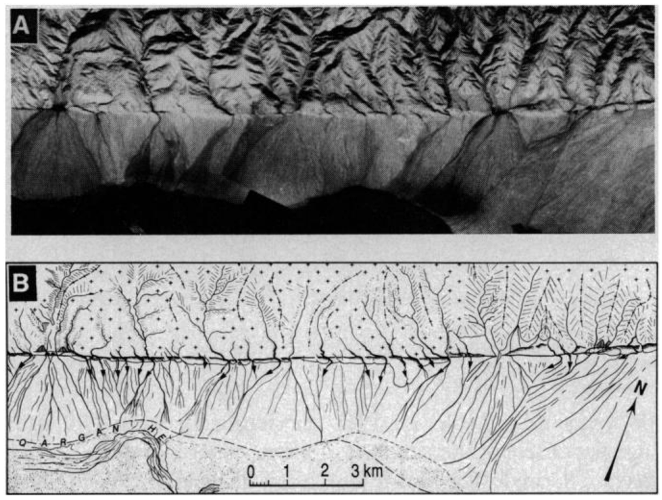

Fig. 3. Image (**A**) and sketch map (**B**) of offset drainage channels near Tura. Site 11 on Fig. 1. Small crosses are for "basement" rock older than Quaternary, other symbols as in Fig. 2. [Panchromatic SPOT scene KJ 221–274]

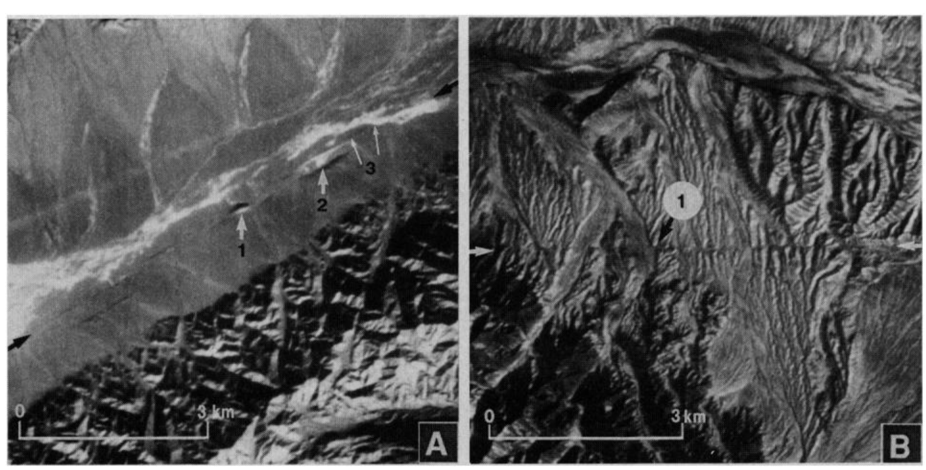

Fig. 4. (**A**) Fault trace across active alluvial fans and silt flats west of Xorkol, site 15. Note compressional (1), and dilational (2), jogs, and 125-m offset of distal edge of small fan (3) [SX Spot scene KJ 229–272]. (**B**) Left-lateral offsets of stream channels along splay of Altyn Tagh fault southwest of Shibaocheng, site 18. Note 60-m offset of eastern edge of large, active channel (arrow 1). Arrows at edges of frames mark fault trace. North is up. [XS SPOT scene KJ 238–271]

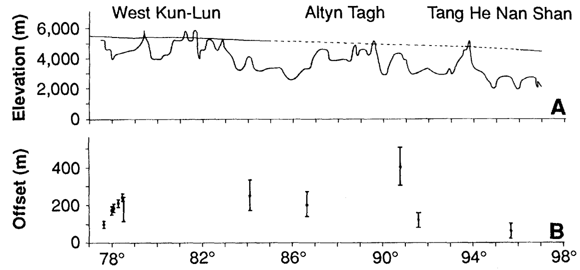

Fig. 5. Diagrams showing (**A**) topographic elevation profile along Altyn Tagh fault between 77° and 97°E, from (6) and present snowline elevation profile, from (12) (dashed when interpolated between 85° and 96°E); (**B**) offsets on the fault at sites discussed in text. Dots with error bars correspond to values listed in Table 1. Large uncertainty (± 100 m) has been assumed for 400 m offset at site 13 because SW edge of fan cannot be defined with precision (10). Vertical bar represents range of ridge offset values at site 7 (10).

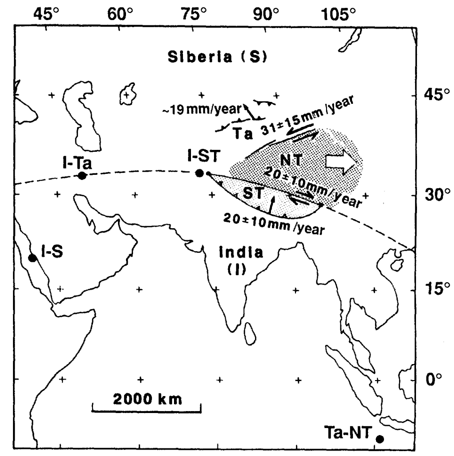

Fig. 6. Diagram showing simplified kinematics of late Quaternary movements induced by penetration of India into Asia in western half of collision zone, where only four major fault zones (thick lines) separate stable or relatively stable (shaded) blocks [after (13), where assumptions are discussed at length and vector diagrams shown]. Ta is Tarim, ST South Tibet, NT North-central Tibet. Black dots are poles of rotations. Thin arrows and associated numbers indicate senses and rates of relative movement. Eastward extrusion of North-central Tibet is shown by large open arrow.

10,000 ± 2,000 years ago (Table 1). We infer a similar age for offsets of the ridges at site 7 and the terrace floored valley at site 2. That the upper and middle terrace levels at site 3 have the same offset, to within the resolution of the images, and that most of the clear offsets in the Karakax valley are between 180 and 240 m (Table 1, Fig. 5), support the hypothesis that the formation of fanglomerates in this valley was an event of comparatively short duration. The variability of the offsets, in turn, probably reflects the finite duration of this event, which, if a result of glacier melting, would not have been catastrophic.

The ages of offsets along the central segment of the Altyn Tagh fault are less certain than in the Karakax valley because the sites are fewer, far apart, and farther from recent glaciers. Because SPOT images reveal no important difference in the morphology of large alluvial fans in the Karakax and Qargan valleys (site 11, Fig. 3) or at site 13, however, we infer that the fans at these distant localities are roughly coeval (10,000 ± 2,000 years) (Table 1). Hence, much of the incision of the now deviated streams that feed the fans at site 11 probably occurred at the beginning of the Holocene (Table 1), [see also (*13*)]. At site 15, the fans and silty deposits offset by the fault are probably only a few thousand years old (Table 1) because they lie in the lowermost, still depositional part of a mountainlocked trough that now collects seasonal waters (Fig. 4A).

Finally, at site 18, the sharpness of the fault trace and the morphology of the erosion channels it cuts appear to be identical to those documented along the east-west strike-slip segment of the Changma fault at Ta Quen Kou (*11*), only 150 km to the northeast. Hence, we assume that the 60 m offset at site 18, which is comparable to the Holocene, 55-m left-lateral offset measured in the field on the Changma fault, is about 10,000 ± 2,000 years old (Table 1).

The morphological evidence unveiled by SPOT thus strengthens the inference that left-lateral movement occurs at fast rates between Tibet and the Tarim Basin. The clustering, between 100 and 400 m of the offset values along the 2000-km-long Altyn Tagh fault (Fig. 5) imply that Holocene horizontal slip rates on the Altyn Tagh fault are a few centimeters per year. Clearly, the Altyn Tagh fault ranks among the largest active strike-slip faults in the world, and may have one of the fastest slip rates among faults of continental Asia.

At a more detailed level, the rate of slip may vary along the fault. We infer that rates of 1.2 ± 0.2 cm per year and 1.5 ± 0.5 cm per year represent lower bounds of the slip rate on the western and central segments of the fault, respectively. From the average value of offsets in the Karakax valley, the most likely rate on the western segment is ~2 cm per year. Offsets along the central, east-northeast striking segment of the fault (between 84° and 92°E) suggest that the rate is higher there, probably ~3 cm per year, because the streams at sites 10 and 11, which are not passive markers, keep straightening their courses and thereby minimize the actual offset measured at the fault (*11*). A rate comparable to that on the Changma fault (~0.5 cm per year) (*11*) appears to characterize the fault splaying from the Altyn Tagh south of Ta Xue Shan. Variations in the rate of slip may reflect the observation that movement near both ends of the Altyn Tagh fault becomes distributed on several easterly striking splays. Left-lateral movement on the fault zone that extends into the Qang Tang platform south of the Karakax valley and joins the Altyn Tagh fault near site 9 (Fig. 1) (*1, 13*) probably combines with movement on the Karakax segment of the fault to yield a rate of horizontal slip faster than 2 cm per year east of the junction. East of Aksay Kazaksu, left-lateral slip at a rate of about 0.5 cm per year on each of the four main splays of the Altyn Tagh fault (Fig. 1), and additional components of thrust motion (*11*) could absorb the more localized 3 cm per year of slip inferred along the central segment of the fault.

The slip rate of ~3 cm per year deduced from the long-term offsets visible on SPOT images along the central segment of the Altyn Tagh fault is similar to that thought to be consistent with the inferred recurrence time and average slip of large earthquakes on this segment at 90°E (3.0 ± 2.0 cm per year) (*4*). Such a rate is also compatible with that predicted from reconstructing first-order movements of crustal blocks between India and Siberia (3.1 ± 1.5 cm per year, Fig. 6) on the basis of the present rate of convergence between these two plates (*16*) and estimates of slip rates between India, South Tibet, and North-central Tibet consistent with observations of Quaternary faulting in southeastern Tibet (*13*). The SPOT images thus support earlier suggestions that extrusion of Tibet toward the east currently absorbs perhaps as much as 30% (*13*) of the crustal shortening induced by the collision between India and Asia. That even the westernmost segment of the Altyn Tagh fault appears to slip at a rate of ~2 cm per year implies that the continuing penetration of India into Asia forces Tibet rapidly toward the east and that strike-slip movements along the edges of Tibet are not a consequence of widespread east-west extension in the Tibetan plateau (*13*).

REFERENCES AND NOTES

1. P. Molnar and P. Tapponnier, *Science* **189**, 419 (1975); P. Tapponnier and P. Molnar, *J. Geophys. Res.* **82**, 2905 (1977).
2. C. Allen, *Geol. Soc. Am. Bull.* **86**, 1041 (1975).
3. Among earthquakes recorded since the turn of the century, only one earthquake of magnitude >7 (3 July 1924) and four earthquakes of magnitude ~6 (12 October 1920, 13 February 1948, 27 December 1951, 28 April 1975) have their epicenters on or

close to the fault [*Catalog of Strong Shocks of China* (Institute of Geophysics Academia Sinica, Beijing, People's Republic of China, 1976)]. Only the 1951 event may be inferred with confidence to correspond to slip on the fault, in view of its focal mechanism (*1*).
4. Molnar and others [P. Molnar *et al.*, *Geology* **15**, 249 (1987); P. Molnar *et al.*, *Science* **235**, 299 (1987)] found large mole tracks and 10-m offsets that they relate to a large earthquake in the last few hundred years on the Altyn Tagh fault near Mangnai Zhen (90°E, Fig. 1). Our fieldwork in the last 3 years has also revealed old earthquake scarps along the fault near Shibaocheng (96°E, Fig. 1). Measurements of scarp profiles imply ages of a few hundred to more than 1000 years.
5. Inferred values of slip rate on the fault range between millimeters and centimeters per year [Ding Guo Yu, *J. Phys. Earth* **34**, S265 (1986); Ma Xing Yuan, *Lithospheric Dynamic Map of China and Adjacent Seas*, scale 1:2,000,000 (State Seismological Bureau, Beijing, China, 1976)].
6. Operational Navigation Charts G7 and G8, scale 1:1,000,000 (Defense Mapping Agency, ed. 3, St. Louis, 1973).
7. The earth observation satellite SPOT (System Probatoire d'Observation de la Terre) was launched on 22 February 1986 by the Centre National d'Etudes Spatiales, France, on a near-polar, circular sunsynchronous orbit, 832 km above the earth's surface. It began commercial operation in July 1986. The scenes used here, 60 km on a side, were provided by SPOT Image, Toulouse, France.
8. Large features of the topography of western Tibet, including the Karakax trough and the glacial morphology of surrounding mountains are clear on Landsat images of the area; see for instance plates E27 and G26 in N. M. Short and R. W. Blair, Jr., Eds., *Geomorphology from Space* (Library of Congress, Washington, DC, 1986).
9. The north and south facing parts of the scarp are respectively shaded from, and illuminated by, the morning sun, Fig. 2C, left.
10. Detailed images of sites not displayed on the figures of this paper are in G. Peltzer, thesis University of Paris VII (1987) and are available from the authors.
11. G. Peltzer *et al.*, *J. Geophys. Res.* **93**, 7793 (1988).
12. B. Wang and E. Derbyshire, *Geogr. J.* **153**, 59 (1987); E. Derbyshire, *Quat. Sci. Rev.* **6**, 301 (1987); *Glacier Inventory of China*, vol. 1 (Lanzhou Institute of Glaciology and Cryopedology, Academia Sinica, Lanzhou, People's Republic of China, 1980).
13. R. Armijo *et al.*, *J. Geophys. Res.* **91**, 13803 (1986); R. Armijo *et al.*, *ibid.* **94**, 2787 (1989).
14. For example, L. D. Labeyrie, J. C. Duplessy, P. L. Blanc, *Nature* **327**, 477 (1987).
15. We take the age of the onset of the Holocene to be between 8,000 and 12,000 years ago, as in (*11*, *13*), because a more precise estimate based on local radiometric dating is not available and unwarranted for our crude estimates.
16. J. B. Minster and T. H. Jordan, *J. Geophys. Res.* **83**, 5331 (1978).
17. We thank SPOT Image, Action Thématique Programmée Télédétection, cosponsored by Centre National de la Recherche Scientifique and Centre National d'Etudes Spatiales, and Programme Tectoscope of Institut National des Sciences de l'Univers for support.

2 June 1989; accepted 11 October 1989.

Structure of a Three-Dimensional, Microporous Molybdenum Phosphate with Large Cavities

Robert C. Haushalter,* Karl G. Strohmaier, Frank W. Lai

The synthesis, single-crystal x-ray structural characterization, and sorption properties of a microporous molybdenum phosphate, $(Me_4N)_{1.3}(H_3O)_{0.7}[Mo_4O_8(PO_4)_2] \cdot 2H_2O$ (Me, methyl), are presented. The three-dimensional framework is built up from $Mo_4O_8^{4+}$ cubes and PO_4^{3-} tetrahedra that are connected in such a way that large, cation-filled voids are generated; these voids constitute 25% of the volume of the solid. Absorption isotherms for water show the completely reversible uptake of 4 to 5 percent by weight water into the micropores of this compound, which corresponds to 10 to 12 percent by volume.

Microporous solids with large internal surface areas, such as zeolites (*1*), find use in such diverse processes as ion exchange, catalysis, and separations. Zeolites, as well as other microporous solids such as the aluminophosphates (*2*) and a recently discovered aluminoborate (*3*), contain frameworks made from *p*-block elements with primarily tetrahedral coordination and are synthesized hydrothermally in the presence of a templating cation. Although certain transition elements can replace some of the tetrahedrally coordinated Si, P, or Al in zeolitic type solids (*4*), similar solids with anionic frameworks containing stoichiometric amounts of octahedrally coordinated transition elements and large organic, cation-filled cavities are not known.

A few iron phosphates, which are naturally occurring or isostructural with known mineral frameworks, have been prepared, with water or alkali metals in the tunnels (*5*), but none have demonstrated microporosity. Since we had synthesized and structurally characterized both solid-state alkali metal molybdenum phosphates, such as $Cs_4Mo_8P_{12}O_{52}$ (*6*), $Cs_4Mo_{10}P_{18}O_{66}$ (*7*), and $Cs_3Mo_4P_3O_{16}$ (*8*), as well as hydrothermally prepared species such as the large cluster $[Na_{14}Mo_{24}P_{17}O_{97}(OH)_{31}]^{6-}$ (*9*) and a one-dimensional (1-D) polymer, $[(H_3O)_2NaMo_6P_4O_{24}(OH)_7]^{2-}$ (*10*), the possibility of preparing a 3-D framework containing voids filled with organic cations seemed reasonable. We report the synthesis and characterization of $(Me_4N)_{1.3}(H_3O)_{0.7}[Mo_4O_8(PO_4)_2] \cdot 2H_2O$, **1**, which contains a metal-metal bonded, 3-D molybdenum phosphate framework whose cation-filled voids constitute 25% of the volume of the solid. Compound **1** is microporous and shows the reversible uptake of 4 to 5% (by weight) water into its pores.

The reaction of MoO_3, Mo (<2 μm particle size), H_3PO_4, $Me_4N \cdot OH$, and H_2O in a mole ratio of 5:1:18:7:165 at 200°C for 3 days gives a nearly quantitative yield of single-phase **1** as a dark red-brown, microcrystalline powder. The powder x-ray diffraction pattern of **1** was indexed as body-centered cubic with a = 15.05(2) Å (the parenthetical number is the error in the last digit), and no systematic absences beyond those due to the body-centering were observed. This result suggested that the structure may be a body-centered relative of the primitive cubic structure of $Cs_3Mo_4P_3O_{16}$ (*8*) (space group, $P\bar{4}3m$), whose a axis is one-half that of **1**. Use of the hydrolysis product of $MoCl_4$ in place of MoO_3 and Mo in the hydrothermal synthesis gives **1** in the form of large, red, single crystals that were used for a crystal structure analysis (*11*).

The 3-D framework of **1** is built up from $Mo_4O_8^{4+}$ cubes, which have four molybdenyl groups (Mo = O) and two metal-metal bonds with a Mo–Mo distance of 2.617(2) Å (Fig. 1A), and PO_4^{3-} tetrahedra in a ratio of 1 to 2 in the cubic space group $I\bar{4}3m$. In this space group, the entire anionic framework in the 3408(1) Å^3 cell is described by just five atoms: the Mo, μ^3-O, and molybdenyl O all lie on Wyckoff g sites at x,x,z; the P atom on the d site ($I\bar{4}$ symmetry) at 1/4,1/2,0; and the μ^2-O on a general position. Each cube has a plane, defined by the surrounding 4/2 phosphate groups (four phosphate groups each shared between two cubes), which is perpendicular to the four molybdenyl Mo–O vectors (Fig. 1, B and C). In the crystals, the $Mo_4O_8^{4+}$ cubes are oriented such that these planes in the z = 0 level are parallel to the (100) plane for the cubes centered around 1/2,0,0 and parallel to the (010) and (001) planes for the cubes centered at 0,1/2,0 and 1/2,1/2,0, respectively (Fig. 2A). At the z = 1/2 level, the phosphate-defined planes for the cubes at 0,0,1/2 and 1/2,0,1/2 are parallel to (001) and (010), respectively (Fig. 2B). This connectivity of the anionic

Exxon Research and Engineering Company, Annandale, NJ 08801.

*To whom correspondence should be addressed.